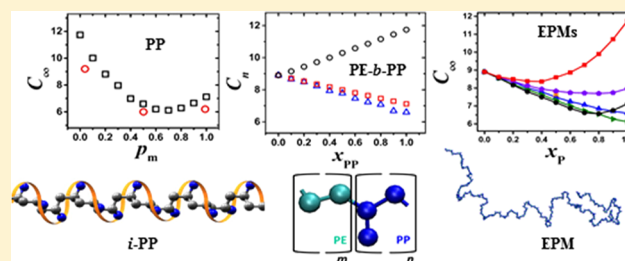


Tacticity Effect on the Conformational Properties of Polypropylene and Poly(ethylene–propylene) Copolymers

Panagiotis-Nikolaos Tzounis,[†] Dora V. Argyropoulou, Stefanos D. Anogiannakis,[‡] and Doros N. Theodorou*[†]

School of Chemical Engineering, National Technical University of Athens, GR 15780 Athens, Greece

ABSTRACT: Tacticity is one of the most important features of stereoregular polymers, with significant impact on morphology and on a variety of properties such as conformational, thermal, rheological, mechanical, etc. In this work we focus on tacticity effects on the conformations and more specifically on the unperturbed dimensions of single polypropylene (PP) homopolymer and both block and random poly(ethylene–propylene) copolymer chains. The equilibration of all chains is achieved by applying the single-chain Monte Carlo algorithm of Tzounis et al. [*Macromolecules* 2017, 50, 4575–4587]. In agreement with past studies, we find that tacticity has a significant effect on the stiffness of PP homopolymer. The characteristic ratio exhibits a nonmonotonic dependence on the fraction of *meso* dyads along the PP chains, which results from two competing mechanisms, revealed by analysis of the torsional states of the PP chain backbones. A simple theoretical model is developed to describe the dependence of the stiffness of poly(ethylene-*block*-propylene) copolymer on its propylene content and on the tacticity of its PP block. Finally, the effect of both tacticity and propylene content on the stiffness of poly(ethylene-*random*-propylene) chains, used to model ethylene–propylene monomer (EPM) materials, is found to be in very good qualitative agreement with available rotational isomeric state (RIS) model predictions.



INTRODUCTION

Tacticity or chirality of polymer chains, which is defined as the arrangement of adjacent chiral centers along a polymer chain, is one of the most important parameters in the design of macromolecules, as it strongly affects the properties of the materials obtained from them. Tacticity is usually identified by the sequence of the so-called dyads, which consist of two sequential chiral units along the polymer chain. There are two kinds of dyads: *meso* (*m*) dyads, consisting of two chiral units of the same stereochemical configuration, and *racemo* (*r*) dyads, where the two chiral units have opposite configurations. Experimentally, the tacticity of macromolecules is usually characterized by ¹³C NMR spectroscopic techniques,^{1–6} while in simulations it is usually identified by geometric criteria.^{7–15}

Tacticity plays a significant role in many properties of polymers. Dynamical properties such as the self-diffusion coefficient D_{cm} ¹⁶ and the glass transition temperature T_g ,^{17–21} rheological properties such as the entanglement molar mass M_e and the plateau modulus G_e ,^{22–27} and the crystallization^{28–30} as well as the permeability³¹ of chiral homopolymers are strongly affected by their tacticity. They have been extensively studied in the literature by both experiments and simulations. Furthermore, the miscibility of various polymer blends^{17,32–43} is determined by the tacticity of the mixed chains. The effect of tacticity on polymer chain miscibility is also reflected in the different microphases in which block copolymers usually self-organize. Different tacticities can lead to the formation of different microphases such as lamellae, cylindrical, hexagonal,

etc., out of copolymers of the same composition.^{44–46} Therefore, tacticity of the blocks is a very important design parameter in block copolymer applications, such as directed self-assembly (DSA) lithography.^{44–48}

Tacticity affects the distribution of torsion angles along the backbones of polymer chains and as a result has a significant influence on chain stiffness. The effect of tacticity on chain stiffness, which is usually quantified through Flory's characteristic ratio, C_∞ , or through the Kuhn length, b , has been a subject of many theoretical and experimental studies. Several theoretical works have extracted the dependence of stiffness on tacticity for various polymers such as polystyrene, poly(methyl methacrylate), and poly(lactide)^{49–53} through rotational isomeric state (RIS) model calculations. Experimentally, the effect of tacticity on the unperturbed dimensions of various polymer chains has been studied through small-angle neutron scattering (SANS) measurements in the melt^{54,55} and intrinsic viscosity measurements in Θ -solutions.^{56,57} The dependence of chain stiffness on tacticity is important because chain stiffness is related to a plethora of polymer properties, such as viscoelastic properties,^{24,58,59} and is also a key input parameter to many coarse-grained models^{60–64} and self-consistent mean-field calculations.^{65–69}

Received: May 25, 2018

Revised: August 5, 2018

Published: August 28, 2018

In this work we choose to systematically study the effects of tacticity on the conformational properties of both homopolymer and copolymer unperturbed chains using single-chain Monte Carlo simulations. Our main target is to identify the microscopic mechanisms through which the chirality of polymer chains affects their stiffness. A very promising candidate in this study was polypropylene (PP) homopolymer due to its simple chemical constitution and the plethora of different conformations it adopts (i.e., 3_1 helical conformation with $s(3/1)1$ symmetry for isotactic, 2_1 helical conformation with $s(2/1)2$ symmetry for syndiotactic, and random coil conformation for atactic).^{27,44,70–72} The stiffness and the conformations of single unperturbed PP chains and their dependence on tacticity at various temperatures have been studied in many works through RIS calculations,^{73–77} and the results have been compared against the corresponding experimental estimates through SANS^{58,78} and/or intrinsic viscosity measurements.⁷⁹ Unfortunately, none of these works provide a microscopic explanation of how tacticity affects stiffness and what are the mechanisms in action. A more comprehensive study of the effect of tacticity on the structure and the dynamics of PP melts was made by Antoniadis et al.^{80,81} Performing molecular dynamics (MD) simulations on isotactic, syndiotactic, and atactic PP melts, they identified the tacticity effects on the glass transition temperature and the segmental dynamics of PP chains. They also performed a systematic analysis of the transitions occurring between different isomeric states as a function of PP chain tacticity, which are mainly responsible for tacticity effects on segmental dynamics.

Apart from PP homopolymers, we also choose to study how tacticity affects the conformational properties of poly(ethylene-*block*-propylene) copolymers and poly(ethylene-*random*-propylene) copolymers, the latter constituting a model for ethylene-propylene monomer (EPM) materials. EPMS are widely used mainly as rubbers in applications such as compatibilizers,⁸² tires,⁸³ electrical and thermal insulations,^{83,84} and pipes.^{83,85} Mark⁸⁶ studied how the unperturbed EPM chain dimensions are affected by both the tacticity and the propylene content using RIS calculations. However, a physical explanation of how propylene content or tacticity affects the stiffness of these random copolymers is still missing. Experimentally, the stiffness of EPMS at various propylene contents is estimated from intrinsic viscosity measurements in Θ -solutions⁸⁷ and SANS measurements^{23,58,88} in polymer melts, but unfortunately, we were unable to find any experimental work which systematically studies how the tacticity of the propylene units would affect the stiffness of EPM chains. However, we found in the literature that the propylene sequences along EPM chains are short; i.e., their average length is approximately 2–2.5 propylene units,^{23,82} suggesting that tacticity should not play a significant role in their conformations. In any case, in the **Results** section, we will also study the impact of the length of propylene unit sequences on EPM chain conformations.

The paper is organized as follows. First we describe in detail the systems we studied and the force field we applied in our simulations. Then, we briefly review the single unperturbed MC simulation methodology we applied to produce long equilibrated MC trajectories of single unperturbed chains. Finally, we present and discuss the results of our study and more specifically (a) the two mechanisms we have identified as affecting the tacticity-dependent stiffness of pure PP chains,

(b) the theoretical model we have developed to link the stiffness of unperturbed poly(ethylene-*block*-propylene) chains with their chemical composition and tacticity, and (c) the dependence of stiffness of poly(ethylene-*random*-propylene) chains on the tacticity of their propylene sequences, based on a statistical analysis of these sequences.

SYSTEMS STUDIED

In this work, we have studied single unperturbed chains of (i) polyethylene (PE), (ii) polypropylene (PP), (iii) poly(ethylene-*block*-propylene) copolymers, henceforth termed PE-*b*-PP, and (iv) random copolymers of ethylene and propylene, termed EPM in the following. The molecular characteristics of these systems are described in detail below.

Polyethylene (PE). Using the Amorphous Builder of the MAPS suite, developed by Scienomics,⁸⁹ we generated an initial configuration for a single linear PE chain whose chemical constitution is $\text{CH}_3\text{--CH}_2\text{--}(\text{CH}_2\text{--CH}_2)_{499}\text{--CH}_3$. In all PE calculations we have applied the Transferrable Potential for Phase Equilibria United Atom (TraPPE-UA) force field,⁹⁰ wherein hydrogen atoms are fused with the carbon atoms to which they are connected. Therefore, the generated PE chain consists of 1001 united atoms (999 CH_2 and 2 CH_3 united atoms). The version of the TraPPE-UA we applied was the one used in the work of Curro and Grest,^{91,92} with a harmonic bond stretching potential instead of fixed bond lengths.

Polypropylene (PP). The next systems we studied were a series of PP chains with various probabilities (fractions) of *meso* dyads, p_m . In particular, beginning from a single isotactic PP (*i*-PP) chain ($p_m = 1$) generated by the Amorphous Builder of the MAPS suite,⁸⁹ we rotated some of its methyl branches to produce ten new PP chains with $p_m = 0.9, 0.8, \dots, 0.0$, where $p_m = 0.0$ and $p_m = 0.5$ correspond to the syndiotactic PP (*s*-PP) and atactic PP (*a*-PP) chains, respectively. All *meso* and *racemo* (tacticity) sequences were Bernoullian. All PP chains were constructed with head-to-tail configurations, where no propylene inversion was allowed. The united-atom force field we applied was that of Curro and Grest,^{91,92} already adopted for PE. All PP chains consisted of 1501 united atoms in total. The backbone of each chain comprised 1001 united atoms (500 CH , 499 CH_2 , and 2 terminal CH_3), while there were 500 methyl substituents. In other words, the chemical constitution of the chains was $\text{CH}_3\text{--}[\text{CH}(\text{CH}_3)\text{--CH}_2]_{499}\text{--CH}(\text{CH}_3)_2$.

Poly(ethylene-propylene) Block Copolymers (PE-*b*-PP). Apart from PE and PP homopolymer chains, we have also generated and studied three series of PE-*b*-PP copolymer chains. Each series consisted of nine PE-*b*-PP chains with mole fraction $x_p = 0.1, 0.2, \dots, 0.9$ propylene units. In the first series all dyads in the PP block are *meso* (*i*-PP block), in the second all are *racemo* (*s*-PP block), and in the last series there are 50% *meso* and 50% *racemo* dyads (*a*-PP block) with Bernoullian tacticity sequences. All PE-*b*-PP chains consist of the same number of backbone bonds $n = 1000$ as the pure PP chains described above. In other words, the chemical constitution of the block copolymer chains was $\text{CH}_3\text{--}(\text{CH}_2\text{--CH}_2)_{500(1-x_p)}\text{--}[\text{CH}(\text{CH}_3)\text{--CH}_2]_{500x_p}\text{--CH}(\text{CH}_3)_2$, for $0 < x_p < 1$. We applied the same force field as used for the pure PE and PP chains.^{91,92} A synopsis of the number of united atoms and the number of ethylene and propylene units of the PE-*b*-PP chains is shown in **Table 1**.

Ethylene-Propylene Random Copolymers (EPMS) and Alternating Ethylene-Propylene Copolymer (*alt*-

Table 1. Synopsis of the Chemical Constitution of PE-*b*-PP, EPM, and *alt*-PEP Systems

x_p	no. of atoms	no. of ethylene units	no. of propylene units
0.1	1051	450	50
0.2	1101	400	100
0.3	1151	350	150
0.4	1201	300	200
0.5	1251	250	250
0.6	1301	200	300
0.7	1351	150	350
0.8	1401	100	400
0.9	1451	50	450

PEP). Finally, we studied five series of EPM chains. Each series consists of nine EPM chains with $x_p = 0.1, 0.2, \dots, 0.9$ propylene units and corresponds to one of the following probabilities of *meso* dyads $p_m = 0, 0.3, 0.5, 0.7, \text{ and } 1$. In addition, a single alternating poly(ethylene-*alt*-propylene) chain (*alt*-PEP) was also generated for comparison purposes. Both EPM and *alt*-PEP chains have the same number of backbone bonds, $n = 1000$, as the PP and PE-*b*-PP chains we described previously. The TraPPE-UA force field was once again applied for all chains.^{91,92} A synopsis of the number of united atoms as well as the number of ethylene and propylene units of both EPM chains and *alt*-PEP chain is shown in Table 1.

METHODOLOGY

As we have already mentioned in the Introduction, the main goal of this work is to study the effect of tacticity on the conformational properties (Flory's characteristic ratio, Kuhn length, etc.) of single unperturbed chains of chiral homopolymers as well as block and random copolymers with various constitutions. The ensembles of single unperturbed chains whose conformational properties were calculated were created and equilibrated by applying the Metropolis Monte Carlo algorithm developed by Tzounis et al.,⁹³ which has been

successfully applied to a variety of polymer systems with different chemical constitution.

The basic idea of the algorithm is that beginning from the initial configuration of a single polymer chain and performing simple Monte Carlo moves, which are being accepted or rejected according to a Metropolis acceptance criterion, the chain can be fully equilibrated and adopt its unperturbed dimensions. In this work, only the *single atom displacement*, *flip atom*, and *rotate strand (pivot)* moves for the backbone atoms and the *flip branch* move for the branches are performed. Because of the fact that only single unperturbed chains and not entangled polymer melt bulk phases are simulated here, there is no need for concerted rotation, configurational bias, or other computationally demanding moves to be applied. On the other hand, the rotate strand (pivot) move, which is not applicable to Monte Carlo simulations of condensed phases, is one of the most effective moves here and is attempted with a high frequency. In particular, for the PP homopolymer and poly(ethylene-propylene) copolymer chains the attempt frequencies are 10% for the *single atom displacement*, 10% for the *flip atom*, 70% for the *rotate strand (pivot)* move applied to the backbone atoms, and 10% for the *flip branch* moves. Especially for the PE chains the attempt frequencies are 10% for the *single atom displacement* move, 10% for the flip atom move, and 80% for the *rotate strand (pivot)* move. In both cases we choose to have high percentages for the *rotate strand (pivot)* move due to the fact that it is the most effective move in decorrelating our single-chain conformations.

The most important feature of the algorithm lies in its treatment of intermolecular nonbonded interactions, which ensures that the sampled polymer chains are indeed unperturbed and representative of those encountered in a melt. According to Flory's definition,⁹⁴ in a single unperturbed chain there are only "local" interactions. The algorithm provides a methodology and a simple criterion to determine the optimum range of intermolecular interactions within which all interactions can be considered as "local". This range is estimated by systematically varying the maximal topological

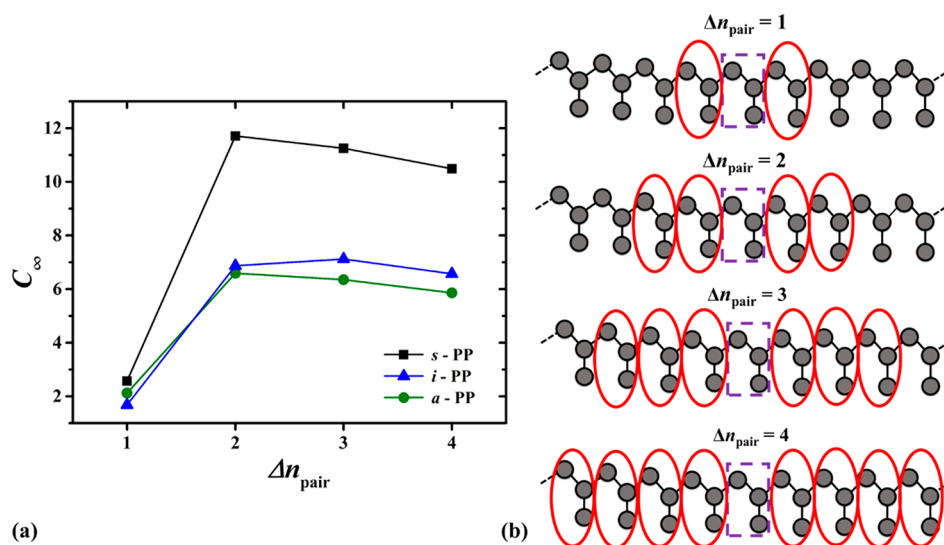


Figure 1. (a) Flory's characteristic ratio, C_∞ , plotted as a function of Δn_{pair} for the syndiotactic ($p_m = 0.0$), atactic ($p_m = 0.5$), and isotactic ($p_m = 1.0$) PP chains. (b) Schematic representation of four PP chains. With red ellipses we mark the monomers whose interactions with the central monomer, indicated with the purple dashed rectangle, are considered as local and therefore taken into account in the MC sampling, for each one of the cases $\Delta n_{\text{pair}} = 1, 2, 3, \text{ and } 4$.

distance of repeat units (Δn_{pair}) between which nonbonded forces are active, until a maximum in stiffness (expressed by Flory's characteristic ratio) is achieved.

As described in the **Systems Studied** section, the initial configurations of the single chains, which are the input of the MC algorithm, were basically generated using the amorphous builder plugin of MAPS suite.⁸⁹ However, the desired probabilities of *meso* dyads (p_m), in both homopolymer and copolymer chains, were achieved by applying a home-built algorithm which alters the generated conformations by rotating the methyl branches, implementing a Bernoullian distribution of dyads, until the desired p_m is reached.

RESULTS AND DISCUSSION

In this section we present and discuss the results of our study of the effect of tacticity on the unperturbed dimensions of PP homopolymer chains as well as of PE-*b*-PP and EPM copolymer chains with various PP contents. Note that in all figures error bars are very small, comparable to the width of the lines, and therefore are omitted.

PP. The first set of systems we studied was a series of PP chains characterized by Bernoullian distribution of dyad types with probability of *meso* dyads $p_m = 0, 0.1, 0.2, \dots, 1.0$. For each system we perform single unperturbed chain MC simulations at constant temperature $T = 450$ K, applying the algorithm we described in the **Methodology** section, for approximately 1 billion MC steps and for different Δn_{pair} values to determine the one where stiffness, expressed by Flory's characteristic ratio, is maximized. In **Figure 1a**, we plot the characteristic ratio C_∞ as a function of Δn_{pair} for the three homopolymer syndiotactic ($p_m = 0.0$), atactic ($p_m = 0.5$), and isotactic ($p_m = 1.0$) PP chains. We note that C_∞ is maximized at $\Delta n_{\text{pair}} = 2$ for the *s*-PP and *a*-PP chains and at $\Delta n_{\text{pair}} = 3$ for the *i*-PP chain. In **Table 2** we show the values of Δn_{pair} which maximize C_∞ for each p_m .

Table 2. Δn_{pair} Values That Maximize C_∞ for Each p_m for the PE and PP Homopolymer Chains

system	p_m	Δn_{pair}	system	p_m	Δn_{pair}	system	p_m	Δn_{pair}
PE	N/A	2	PP	0.3	2	PP	0.7	3
PP	0.0	2	PP	0.4	2	PP	0.8	3
PP	0.1	2	PP	0.5	2	PP	0.9	3
PP	0.2	2	PP	0.6	2	PP	1.0	3

In **Figure 2**, we plot Flory's characteristic ratio, $C_n = \frac{\langle R^2 \rangle}{nl^2}$, where $\langle R^2 \rangle$ is the mean-square end-to-end distance of a single unperturbed chain, n is the number of backbone bonds, and $l = 1.54$ Å is the average backbone bond length, as a function of n , for a pure PE chain and three PP chains with three different tacticities: an isotactic PP ($p_m = 1$), a syndiotactic PP ($p_m = 0$), and an atactic PP ($p_m = 0.5$). The curves of PE, *s*-PP, and *a*-PP, shown with red, black, and green lines, correspond to a value of $\Delta n_{\text{pair}} = 2$, while the one of *i*-PP, shown with a blue line, corresponds to $\Delta n_{\text{pair}} = 3$. In the limit of long chains ($n \rightarrow \infty$), $\langle R^2 \rangle \sim n$, and C_n reaches a plateau value, C_∞ , for each polymer.

We note that the *s*-PP chain is the stiffest of all with $C_\infty = 11.71$, while the stiffnesses of both *i*-PP ($C_\infty = 7.12$) and *a*-PP chains ($C_\infty = 6.59$) are much smaller and close to each other. Qualitatively, these estimates of the stiffness of PP chains are in agreement with experimental results from SANS measurements,^{58,95,96} according to which *s*-PP ($C_\infty = 9.12$) is much

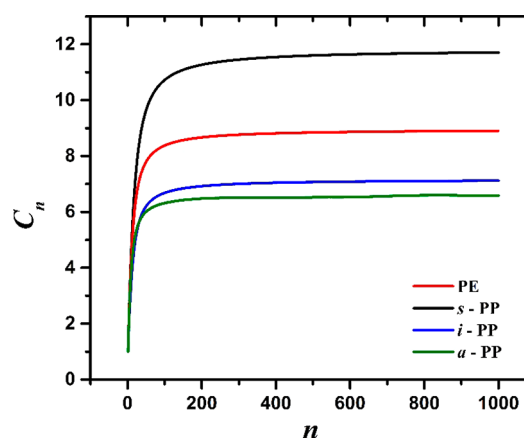


Figure 2. Flory's characteristic ratio, C_n , plotted as a function of the number of backbone bonds, n , for PE, *s*-PP, *a*-PP, and *i*-PP at 450 K.

stiffer than both *i*-PP ($C_\infty = 6.2$) and *a*-PP ($C_\infty = 6.0$), while the last two are close to each other with *i*-PP being a little stiffer than *a*-PP. However, quantitatively, all C_∞ values are overestimated by our simulation in comparison with the experimental ones; this is especially true of the C_∞ value of *s*-PP. The overestimation is in all likelihood due to the TraPPE-UA force field we apply and, more specifically, to its torsional potential, which strongly affects the stiffness of polymer chains. In the previous work of Tzounis et al.⁹³ the stiffness of *i*-PP using the same MC algorithm and at the same temperature, but this time applying the hybrid force field proposed by Logotheti and Theodorou,^{97–99} was estimated as $C_\infty = 5.9$,⁹³ smaller than the one we calculate here and closer to the experimental value.

For comparison, we have also calculated the stiffness of a single unperturbed PE chain using the TraPPE-UA force field. We note that the red curve in **Figure 2**, which corresponds to PE chain, lies between the curves for *s*-PP and *i*-PP. From the plateau value we can estimate $C_\infty = 8.9$ for PE, higher than the estimate of $C_\infty = 8.2$ reported by Tzounis et al.,⁹³ where the anisotropic united-atom (AUA) torsional potential proposed by Toxvaerd¹⁰⁰ was applied, using the same MC algorithm. This overestimation of characteristic ratios for PE by the TraPPE-UA force field is well-known in the literature^{92,101,102} and has recently been discussed in detail in the work of Ramos et al.,¹⁰³ where a comprehensive review of the estimation of various physical and thermodynamic quantities of PE through computer simulations is presented.

In **Figure 3**, we plot the modified persistence length: $\langle l_p^{(k)} \rangle \equiv \left\langle \frac{\mathbf{r}_k \cdot \mathbf{R}}{|\mathbf{r}_k|} \right\rangle$, as defined in the works of Connolly et al.^{104,105} and Yethiraj et al.,¹⁰⁶ where \mathbf{R} is the end-to-end vector of the chain and \mathbf{r}_k is the bond vector of the k -th backbone bond versus k for the *s*-PP and *i*-PP chains. Note that $k = 1$ refers to the first backbone bond of the chain, and therefore $\langle l_p^{(1)} \rangle$ corresponds to the original Flory definition of persistence length. Because of the fact that in this type of plot for each k value only a single value of $l_p^{(k)}$ is obtained from a given unperturbed chain configuration, a very large sample of single unperturbed PP chains is needed to reduce the noise of the plot. For this reason we limit this analysis only to the *s*-PP ($p_m = 0$) and *i*-PP ($p_m = 1$) chains. In **Figure 3**, chain end effects on the conformation and the tacticity of PP chains are clearly reflected. We note that $\langle l_p^{(k)} \rangle$ displays a strong dependence on k near chain ends, but at approximately $k = 50$ and $k = 950$ (i.e.,

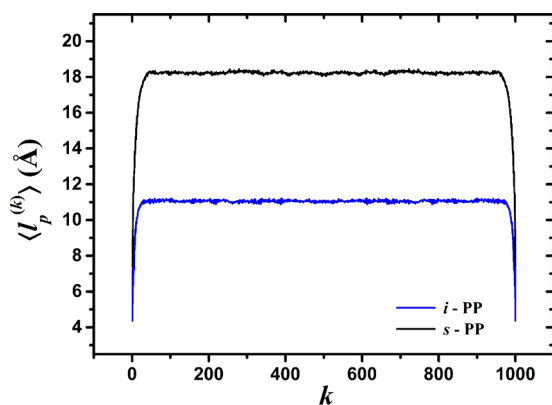


Figure 3. Modified persistence length ($\langle l_p^{(k)} \rangle$) plotted as a function of the index number of the backbone bond vector k for the s -PP and i -PP chains.

50 backbone bonds far from chain ends) it reaches an asymptotic value. This behavior is in agreement with the one shown in Figure 2, where Flory's characteristic ratio, C_m , reaches its plateau value at approximately $n = 100$ backbone bonds.

To investigate systematically how tacticity affects the stiffness of PP chains, we plot C_∞ as a function of the probability of *meso* dyads, p_m , in Figure 4 (black squares). A

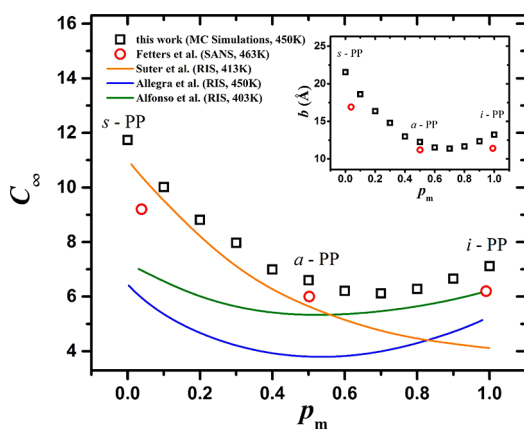


Figure 4. Characteristic ratio, C_∞ , as a function of the probability of *meso* dyads, p_m , for the PP homopolymer chains. Black squares correspond to our simulation results, and red circles correspond to the experimental values in the work of Fetters et al.^{58,95,96} The orange, green, and blue curves correspond to the RIS calculations of Suter and Flory,⁷⁴ Alfonso et al.,¹⁰⁹ and Allegra et al.,¹⁰⁸ respectively. In the inset the statistical (Kuhn) segment length, b , is plotted as a function of the probability of *meso* dyads, p_m . Black squares correspond to our simulation results, while red circles correspond to the experimental measurements of Fetters et al.^{58,95,96}

schematic representation of a *meso* (m) and a *racemo* (r) PP dyad, m , is shown in Figure 5a. We note that the dependence of C_∞ on p_m is not monotonic and a minimum stiffness appears at approximately $p_m = 0.7$. As expected, the same behavior is also present in the inset of Figure 4, where the Kuhn length $b = \frac{\langle R^2 \rangle}{nl \cos(\theta/2)} = \frac{C_\infty l}{\cos(\theta/2)}$, with $\pi - \theta$ being the average angle between two sequential backbone bonds, is plotted versus p_m . At approximately $p_m = 0.7$ there is a minimum of b which corresponds to the minimum stiffness. Because of the lack of experimental measurements of C_∞ for various p_m , except those

for $p_m = 0.0385$ ²⁷ for s -PP, 0.502 ¹⁰⁷ for a -PP, and 0.9905 ²⁷ for i -PP, denoted by red circles in Figure 4, we choose to compare our estimations with the results obtained from theoretical rotational isomeric state (RIS) model calculations,^{74,108,109} shown in Figure 4 as colored lines. The same nonmonotonic behavior is also evident in the works of Allegra et al.¹⁰⁸ and Alfonso et al.,¹⁰⁹ who found a minimum C_∞ value at approximately $p_m = 0.45$ and 0.57 , respectively. On the other hand, Suter and Flory⁷⁴ predicted a monotonic decrease of C_∞ as p_m increases. Furthermore, for $p_m \leq 0.5$ our estimates for C_∞ are in good agreement with the values calculated in the work of Suter and Flory,⁷⁴ while for $p_m > 0.5$ they progressively deviate from that work and are in good agreement with the ones calculated by Alfonso et al.¹⁰⁸

Unfortunately, none of the above-mentioned theoretical works provide a physical explanation regarding the appearance of a minimum stiffness. In this direction, we performed an analysis of the single unperturbed PP chain conformations we simulated, based on the torsional state sequences of their backbones. First of all, we extract the normalized distributions of torsion angles along the backbone of the PP chains, shown in Figure 6a, and we identify the three torsional states, *trans* (t), *gauche* (g), and *gauche bar* (\bar{g}). In particular, the *gauche bar* (\bar{g}) state corresponds to the torsional angle range $0^\circ \leq \varphi < 125^\circ$, the *trans* (t) state to $125^\circ \leq \varphi < 245^\circ$, and finally the *gauche* (g) state to $245^\circ \leq \varphi \leq 360^\circ$. The bounds of the ranges we use are determined from the minima of the normalized distributions of Figure 6a, i.e., $\varphi = 0^\circ$, 125° , 245° , and 360° correspond to the first, second, third, and fourth minima of the distributions. The definitions of these torsional states using Newman projections are shown in Figure 5b. Here, we should mention that in the RIS model for PP developed by Suter and Flory⁷⁴ five torsional states are defined, i.e., *trans* (t), *trans star* (t^*), *gauche* (g), *gauche star* (g^*), and *gauche bar* (\bar{g}). In our continuous simulations, *trans star* (t^*) and *gauche star* (g^*) are merged with *trans* (t) and *gauche* (g), respectively, giving rise to the corresponding asymmetric *trans* (t) and *gauche* (g) peaks. The same behavior is evident in other works with continuous simulations, either MC or MD, of PP melt chains.^{80,81,97}

We notice that as p_m decreases (moving from i -PP to s -PP) the probability of the *trans* state increases, while the probability of the *gauche* (g) state decreases, both indicating that PP chains become stiffer, with higher characteristic ratios. On the other hand, *gauche bar* (\bar{g}) probabilities are very small, almost negligible, due to the fact that *gauche bar* states are energetically unfavorable. Figure 6a provides no evidence of a nonmonotonic behavior such as the one we show in Figure 4. In view of this, we continue our analysis by calculating, in Figure 6b, the average percentages of *trans*, p_t , and *gauche*, p_g , torsional angles as a function of p_m . We note that as p_m increases (moving from s -PP to i -PP) p_t decreases and p_g increases, as expected from the distributions of Figure 6a. Around $p_m = 0.7$ (marked by a dashed vertical line), which corresponds to the probability where the minimum stiffness appears in Figure 4, we simulated and analyzed PP chains with $p_m = 0.62, 0.64, \dots, 0.9$ to easily track any change in the behavior of p_t and p_g . Unfortunately, there is no noticeable change in the slope of either curve. Similar behavior is observed in Figure 6c, where the fractions of tt , gg , and tg pairs of torsion angles, p_{tt} , p_{gg} , and p_{tg} , respectively, are plotted against p_m (gt pairs are lumped together with tg pairs). In the inset of Figure 6c, where a zoomed version of the p_{gg} versus p_m

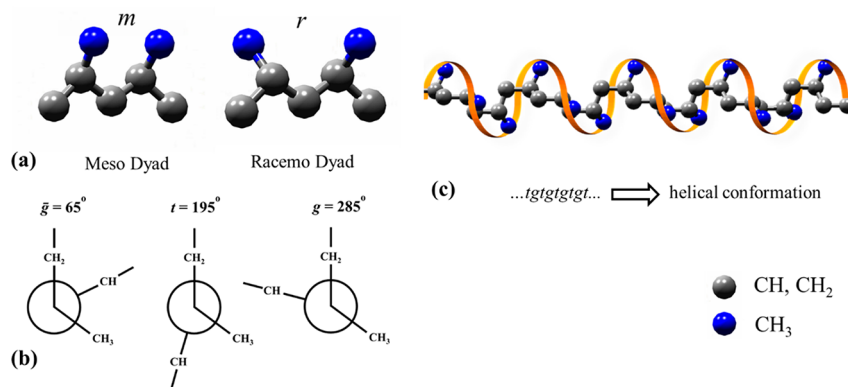


Figure 5. (a) Schematic representation of a *meso*, m , and a *racemo*, r , PP dyad. (b) Newman projections of three states \bar{g} , t , and g . (c) Snapshot of helical conformation of i -PP chain, which corresponds to the $t g t g t g \dots$ torsional state sequence.

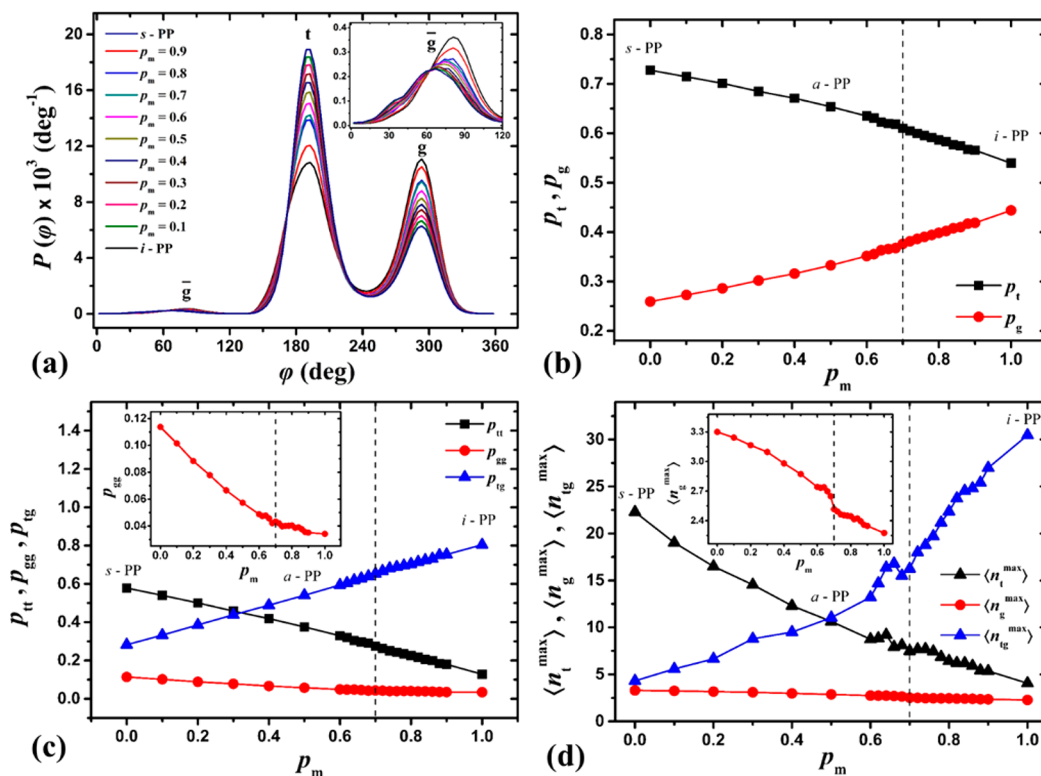


Figure 6. (a) Normalized backbone torsional angle distributions for PP chains with different probabilities of *meso* dyads, $p_m = 0, 0.1, \dots, 1$. *Trans* (t), *gauche* (g), and *gauche bar* (\bar{g}) states have been identified. A zoom into the \bar{g} peak is shown in the inset of the plot. (b) Average fractions of *trans*, p_t , and *gauche*, p_g , states versus p_m denoted with black and red lines and symbols, respectively. (c) Fractions of tt (p_{tt}), gg (p_{gg}), and tg (p_{tg}) pairs of torsion angles versus p_m . In the inset a zoomed p_{gg} versus p_m is shown. (d) Average maximum length, expressed in number of torsion angles, of all-*trans* ($\langle n_t^{\max} \rangle$), all-*gauche* ($\langle n_g^{\max} \rangle$), and all-*trans-gauche* ($\langle n_{tg}^{\max} \rangle$) sequences along the backbone of PP chains versus p_m . In the inset a zoomed $\langle n_{tg}^{\max} \rangle$ versus p_m plot is shown.

plot is shown, one can notice a small change in the slope at $p_m = 0.7$. Finally, in Figure 6d we plot the average maximum lengths, expressed in number of torsion angles, of all-*trans* ($tttt\dots$), all-*gauche* ($ggggg\dots$), and all-*trans-gauche* ($tgtgtg\dots$) sequences $\langle n_t^{\max} \rangle$, $\langle n_g^{\max} \rangle$, and $\langle n_{tg}^{\max} \rangle$, respectively, versus p_m . As expected, as we move from s -PP to i -PP (with increasing p_m), $\langle n_t^{\max} \rangle$ decreases; i.e., all-*trans* sequences become shorter on average, leading to less stiff PP conformations. In addition, as p_m increases, $\langle n_g^{\max} \rangle$ decreases, i.e., all-*gauche* sequences become shorter; in general, $ggggg\dots$ sequences are not favorable, as reflected by the low values of $\langle n_g^{\max} \rangle$. In $\langle n_t^{\max} \rangle$ there is a monotonic behavior, while in $\langle n_{tg}^{\max} \rangle$ there is a noticeable

change in the slope at $p_m = 0.7$, similar to the one shown in the inset of Figure 6c. However, the changes in the slopes of the corresponding plots we observed so far are only indications that a change in the conformation of PP chains occurs around $p_m = 0.7$ but do not provide a concrete physical interpretation.

A very informative quantity that will aid us in the direction of providing a physical meaning and uncovering the origins of minimum stiffness appearing in Figure 4 is $\langle n_{tg}^{\max} \rangle$ which, as mentioned above, is plotted with blue line and symbols in Figure 6d and refers to the maximum length of $tgtgtg\dots$ sequences along the backbone of PP chains. These sequences correspond to a *helical conformation* of the PP chain, as shown

Table 3. Probabilities of Triads of Torsional States

sequence	p_m										
	0.0	0.1	0.2	0.3	0.4	0.5	0.6	0.7	0.8	0.9	1.0
<i>ttt</i>	0.44	0.40	0.35	0.30	0.26	0.22	0.17	0.13	0.12	0.06	0.03
<i>ttg, gtt</i>	0.25	0.28	0.29	0.30	0.31	0.31	0.31	0.29	0.28	0.23	0.19
<i>tgt</i>	0.03	0.07	0.11	0.15	0.18	0.22	0.25	0.28	0.29	0.34	0.37
<i>tgg, ggt</i>	0.21	0.18	0.16	0.14	0.12	0.10	0.08	0.08	0.07	0.06	0.06
<i>gtg</i>	0.01	0.03	0.04	0.18	0.09	0.11	0.14	0.18	0.19	0.26	0.30
<i>ggg</i>	0.01	0.01	0.01	0.01	0.01	0.01	0.01	0.01	0.00	0.01	0.00

Table 4. Probabilities of Tetrads of Torsional States

sequence	p_m										
	0.0	0.1	0.2	0.3	0.4	0.5	0.6	0.7	0.8	0.9	1.0
<i>tttt</i>	0.35	0.30	0.25	0.20	0.16	0.13	0.09	0.06	0.05	0.02	0.01
<i>tttg, gttt</i>	0.17	0.19	0.19	0.19	0.19	0.17	0.16	0.13	0.12	0.08	0.04
<i>ttgt, tgtt</i>	0.06	0.11	0.16	0.19	0.23	0.24	0.26	0.25	0.25	0.21	0.17
<i>tgtg, gtgt</i>	0.01	0.03	0.06	0.10	0.13	0.18	0.24	0.31	0.33	0.47	0.55
<i>ttgg, gggt</i>	0.19	0.16	0.13	0.10	0.08	0.06	0.05	0.04	0.03	0.02	0.02
<i>tggt</i>	0.10	0.09	0.07	0.06	0.05	0.04	0.04	0.03	0.03	0.03	0.03
<i>gttg</i>	0.04	0.04	0.05	0.05	0.06	0.07	0.07	0.08	0.08	0.08	0.07
<i>tggg, gggg</i>	0.01	0.01	0.01	0.01	0.01	0.01	0.01	0.01	0.01	0.01	0.01
<i>gtgg, gggt</i>	0.01	0.02	0.03	0.03	0.04	0.04	0.04	0.04	0.04	0.04	0.04
<i>gggg</i>	0.00	0.00	0.00	0.00	0.00	0.00	0.00	0.00	0.00	0.00	0.00

Table 5. Probabilities of Pentads of Torsional States

sequence	p_m										
	0.0	0.1	0.2	0.3	0.4	0.5	0.6	0.7	0.8	0.9	1.0
<i>ttttt</i>	0.27	0.22	0.17	0.13	0.10	0.07	0.05	0.03	0.03	0.01	0.00
<i>ttttg, gtttt</i>	0.16	0.15	0.14	0.13	0.12	0.11	0.09	0.06	0.06	0.03	0.01
<i>ttttg, tgttt</i>	0.04	0.08	0.11	0.13	0.14	0.14	0.13	0.11	0.11	0.07	0.04
<i>tttgg, ggttt</i>	0.13	0.10	0.08	0.06	0.04	0.03	0.02	0.02	0.10	0.01	0.00
<i>ttgtt</i>	0.02	0.04	0.06	0.06	0.07	0.07	0.06	0.05	0.05	0.03	0.02
<i>ttgtg, gttgt</i>	0.01	0.03	0.05	0.06	0.09	0.10	0.12	0.14	0.14	0.14	0.13
<i>ttggt, tgggt</i>	0.18	0.15	0.12	0.10	0.07	0.05	0.04	0.03	0.03	0.02	0.01
<i>ttggg, ggggt</i>	0.01	0.01	0.01	0.01	0.01	0.01	0.01	0.00	0.00	0.00	0.00
<i>tgttg, gttgt</i>	0.01	0.03	0.05	0.07	0.09	0.10	0.12	0.13	0.13	0.14	0.13
<i>tgtgt</i>	0.00	0.01	0.02	0.03	0.05	0.07	0.10	0.14	0.15	0.21	0.25
<i>tgtgg, ggtgt</i>	0.01	0.02	0.03	0.03	0.03	0.03	0.03	0.03	0.03	0.04	0.04
<i>tgtgtg, gttgtg</i>	0.01	0.02	0.03	0.03	0.03	0.03	0.03	0.03	0.03	0.03	0.04
<i>tgggt</i>	0.00	0.00	0.00	0.00	0.00	0.00	0.00	0.00	0.00	0.00	0.00
<i>tgggg, ggggt</i>	0.01	0.01	0.00	0.00	0.00	0.00	0.00	0.00	0.00	0.00	0.00
<i>gtttg</i>	0.01	0.02	0.02	0.03	0.03	0.03	0.03	0.03	0.03	0.02	0.02
<i>gttgg, ggttg</i>	0.06	0.06	0.05	0.04	0.03	0.03	0.02	0.02	0.02	0.01	0.01
<i>gtgtg</i>	0.00	0.00	0.01	0.01	0.02	0.04	0.06	0.08	0.09	0.16	0.21
<i>gtggg, ggggt</i>	0.00	0.00	0.00	0.00	0.00	0.00	0.00	0.00	0.00	0.00	0.00
<i>ggttg</i>	0.00	0.00	0.00	0.00	0.00	0.00	0.00	0.00	0.00	0.00	0.00
<i>ggggg</i>	0.00	0.00	0.00	0.00	0.00	0.00	0.00	0.00	0.00	0.00	0.00

in Figure 5c. We note that the average length of such helical sequences increases progressively with p_m , but at $p_m = 0.7$ there is an abrupt change in the slope of $\langle n_{ig}^{\max} \rangle$ with p_m , indicating that there are long enough segments with helical conformations present along the PP chain backbones to bring about an increase in the overall stiffness of the chains. Combining the latter microscopic picture with the fact that all-*trans* sequences become shorter (and also both p_t and p_{tt} decrease) as p_m increases, we can conclude that there are *two* opposing processes acting simultaneously and determining how tacticity affects PP stiffness. In the first process, as one moves from *s*-PP to *i*-PP, the population of *trans*-states and, therefore the

average length of all-*trans* sequences, decrease, leading to less stiff conformations. However, at the same time, more and more lengthy *helical conformations* (*tgtgtg...*) appear, tending to increase the stiffness of the chains. The first process dominates at $p_m \leq 0.7$, causing C_∞ to decrease as p_m increases (see Figure 4). The second process dominates for $p_m > 0.7$, causing C_∞ to increase as p_m increases. Clearly, the value of p_m where the second process begins to affect the stiffness of PP chains, if at all, depends on the force field we invoke to describe the interactions of PP atoms. In the RIS models of Alfonso et al.¹⁰⁸ and Allegra et al.¹⁰⁷ the second process begins to act at $p_m \approx 0.5$, lower than our estimate. On the other hand, in the RIS

model of Suter and Flory⁷⁴ the second process is unable to cause a noticeable change in stiffness, and the first process dominates for all p_m values.

We have extended our analysis to longer sequences. In Tables 3, 4, and 5 we show the probabilities of all possible triads, tetrads, and pentads formed from the dominant t and g torsional states for various p_m values. In each column of the tables the probabilities do not add up to 1 because sequences involving the improbable \bar{g} torsional state have not been included. In all tables we mark in bold the sequences of torsional states which correspond to the two highest probabilities. For low p_m values ($p_m < 0.3$), i.e., as we approach s -PP, the most favorable triad is ttt , consisting of sequential *trans* states. On the other hand, for higher p_m values ($p_m > 0.7$), i.e., as we approach i -PP, the most favorable triad is tgt , a part of the helical conformation $tgtgtgtg\dots$. Similarly, the most favorable tetrads and pentads of torsional states for $p_m < 0.3$ are $tttt$ and $ttttt$, while for $p_m > 0.7$ they are $tgtg$ and $tgtgt$, respectively. The analysis of higher order sequences of torsional states, such as triads, tetrads, and pentads, provides further evidence for the two opposing mechanisms which act together and were described previously. One could ask the question, which of the sequence lengths we have analyzed is the most impactful, i.e., better reflects the conformational preferences induced by the stereo sequence, while at the same time not being too long. The answer, in our opinion, is the tetrads. The contrast between the probabilities of the two most preferable tetrad sequences and the rest is higher than the corresponding contrast for triads or pentads. For example, in i -PP ($p_m = 1.0$) the probability of the $tgtg$ tetrad, $p_{tgtg} = 0.55$, is very high compared to the probabilities of all other sequences. Similar behavior is observed for other tacticities, p_m . This contrast is less strong in pentads probably due to the higher number of sequences that can be adopted.

Finally, in Figure 7 we calculate the temperature coefficient, $\kappa = \frac{d \ln(C_\infty)}{dT}$ as a function of p_m , denoted with black squares. κ is predicted to be negative. The behavior with p_m is once again nonmonotonic, with a minimum in $|\kappa|$ appearing at approximately $p_m = 0.40$. We compare our results with the

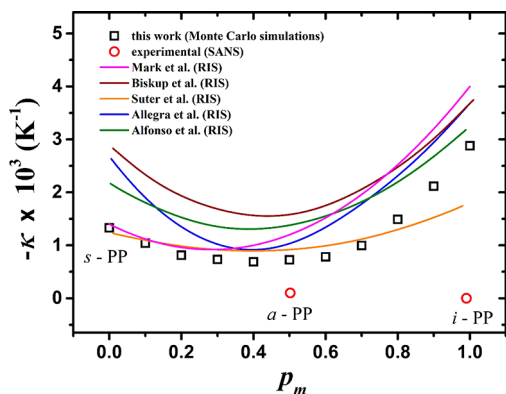


Figure 7. Temperature coefficient, κ , versus the probability of meso dyads, p_m , of a series of PP chains. Black squares correspond to our simulation results and red circles to the experimental measurements using SANS.^{95,110} Colored lines correspond to estimations from various RIS theoretical works and in particular the pink line to Mark,⁸⁶ the brown line to Biskup et al.,⁷³ the orange line to Suter and Flory,⁷⁴ the blue line to Allegra et al.,¹⁰⁸ and the green line to Alfonso et al.¹⁰⁹

calculations of various RIS models, displayed with colored lines. RIS models also predict a minimum value of $|\kappa|$ at $p_m = 0.30$ – 0.50 , which is in good agreement with our estimations. However, our $|\kappa|$ values are underestimated compared to RIS predictions,^{73,74,86,108,109} possibly due to the TraPPE-UA force field we apply. On the other hand, experimental measurements using SANS^{95,110} do not betray any significant temperature dependence of C_∞ ($\kappa = -0.1$ for a -PP and $\kappa = 0$ for i -PP); unfortunately, we were unable to find any experimental results for other PP tacticities.

PE- b -PP. In this section we study the effect of tacticity on the stiffness of PE- b -PP copolymer chains with various propylene contents. A 3D representation of a PE- b -PP chain consisting of 500 ethylene and 500 propylene units ($x_p = 0.5$) is shown in Figure 8, where the PE and PP blocks are denoted

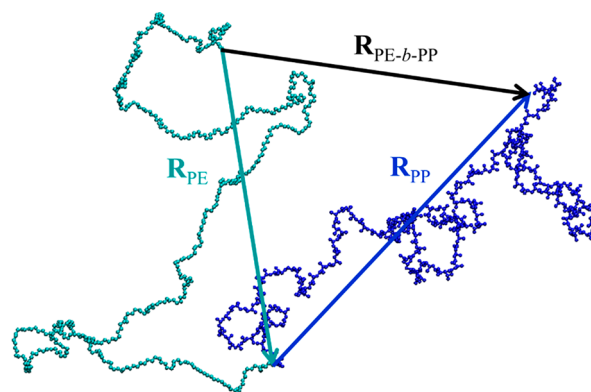


Figure 8. Schematic representation of end-to-end vectors on an unperturbed chain of PE- b -PP consisting of 500 ethylene and 500 propylene units denoted with cyan and blue colors, respectively. The cyan vector corresponds to the end-to-end vector of PE block, R_{PE} , the blue vector to the end-to-end vector of PP block, R_{PP} , and finally the black vector to the end-to-end vector $R_{PE-b-PP}$ of the whole PE- b -PP chain.

with cyan and blue colors, respectively. As we described in the Systems Studied section, we generate three series of PE- b -PP chains with $p_m = 0, 0.5$, and 1.0 . Each series consists of nine PE- b -PP chains with $x_p = 0.1, 0.2, \dots, 0.9$. In the end we have 27 PE- b -PP chains with various x_p and p_m values. We choose all PE- b -PP chains to have the same backbone length as the PE and PP homopolymer chains we simulated and studied in the previous section, i.e. $n = 1000$ backbone bonds.

For each system we perform single unperturbed chain MC simulations, at constant temperature $T = 450$ K, applying the algorithm we described in the Methodology section, for approximately 1 billion MC steps. Here, we use for each PE or PP block the optimum Δn_{pair} value we estimated from the simulations of the corresponding PE and PP homopolymers, shown in Table 2.

In Figure 9a–c, we plot with black squares the characteristic ratio of the block copolymer, $C_n^{\text{PE-}b\text{-PP}}$, as a function of x_{PP} for $p_m = 0, 0.5$, and 1.0 , respectively. Here, x_{PP} corresponds to the mole fraction of the PP block backbone bonds:

$$x_{PP} = \frac{n_{PP}}{n_{PP} + n_{PE}} \quad (1)$$

where n_{PP} and n_{PE} are the numbers of PP and PE block backbone bonds, respectively, and $n = n_{PP} + n_{PE}$ is the number of backbone bonds in total. We have also added the estimated

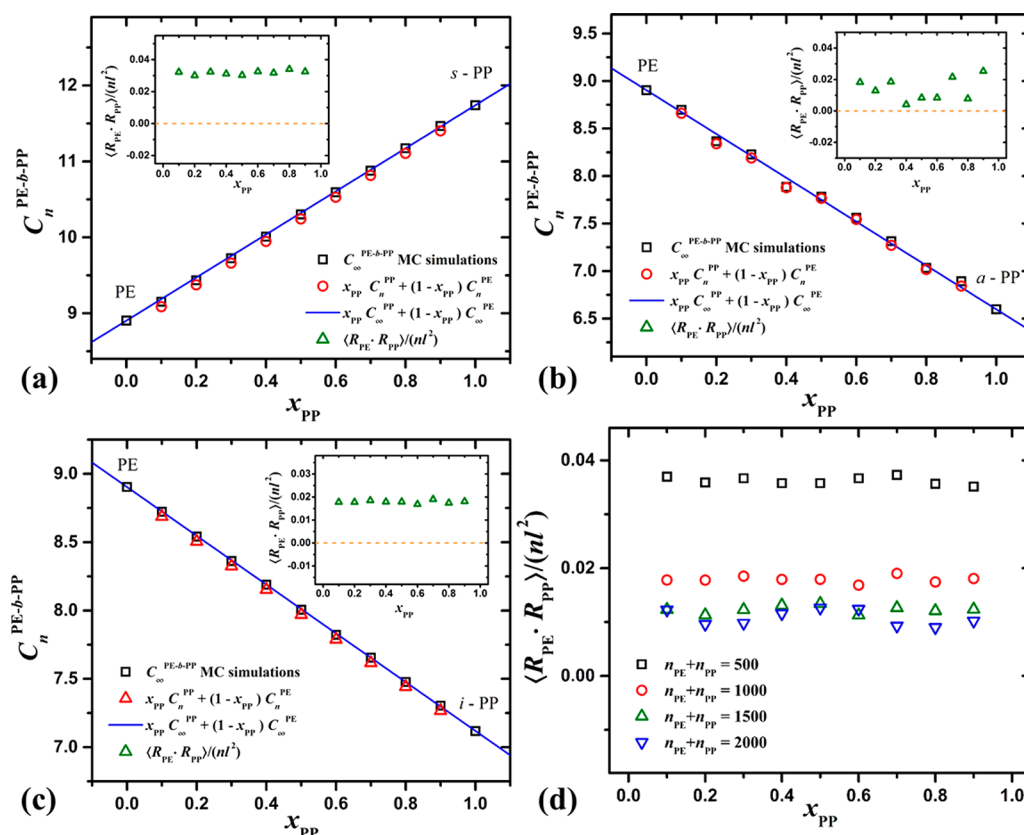


Figure 9. Characteristic ratio, C_∞ , as a function of the mole fraction of the PP block backbone bonds, x_{PP} , for PE-*b*-PP copolymer chains with (a) syndiotactic ($p_m = 0$), (b) atactic ($p_m = 0.5$), and (c) isotactic ($p_m = 1.0$) propylene dyads. Black squares correspond to our estimates of C_n from the MC simulations we performed. Red circles correspond to the estimated values using eq 5. Blue solid lines correspond to the predictions of the theoretical model we developed in eq 6. Green triangles in the insets of (a–c) correspond to the quantity $\langle \mathbf{R}_{PE} \cdot \mathbf{R}_{PP} \rangle / (nl^2)$ versus x_{PP} . (d) Dependence of $\langle \mathbf{R}_{PE} \cdot \mathbf{R}_{PP} \rangle / (nl^2)$ on the molar fraction of the isotactic PP block backbone bonds, x_{PP} , for various copolymer chain lengths.

C_∞ values of PE ($x_{PP} = 0$) and of *s*-PP, *a*-PP, or *i*-PP ($x_{PP} = 1$) which correspond to $p_m = 0, 0.5$, and 1.0 , respectively. We should note that for $x_{PP} = 0$ where $n_{PE} = n$ the characteristic ratio of the PE block $C_{n_{PE}}^{PE} = C_\infty^{PE}$. In addition, for $x_{PP} = 1$, where $n_{PP} = n$, the characteristic ratio of the PP block $C_{n_{PP}}^{PP} = C_\infty^{PP}$ for all three tacticities. However, as we will discuss below, for $0 < x_{PP} < 1$ the characteristic ratios $C_{n_{PE}}^{PE}$ and $C_{n_{PP}}^{PP}$ of the PE and PP blocks satisfy $C_{n_{PE}}^{PE} \leq C_\infty^{PE}$ and $C_{n_{PP}}^{PP} \leq C_\infty^{PP}$, respectively, because PE and PP blocks are not long enough and both $C_{n_{PE}}^{PE}$ and $C_{n_{PP}}^{PP}$ have not reached a plateau value yet.

In all Figure 9a–c, we notice a monotonic increase or decrease of $C_n^{PE-b-PP}$ as a function of x_{PP} , depending on whether C_∞^{PE} is smaller or greater than C_∞^{PP} . For example, in Figure 9a, $C_\infty^{PE} < C_\infty^{s-PP}$ and $C_n^{PE-b-PP}$ increases monotonically with x_{PP} .

Another interesting feature of Figure 9a–c is that $C_n^{PE-b-PP}$ curves follow a very close to linear behavior. To examine this effect and possibly find a model to describe it, we begin from the very definition of the Flory's characteristic ratio $C_n^{PE-b-PP}$, for a PE-*b*-PP copolymer chain, which consists of $n = n_{PP} + n_{PE}$ backbone bonds in total:

$$C_n^{PE-b-PP} = \frac{\langle \mathbf{R}_{PE-b-PP}^2 \rangle}{nl^2} = \frac{\langle (\mathbf{R}_{PE} + \mathbf{R}_{PP})^2 \rangle}{nl^2} = \frac{\langle \mathbf{R}_{PE}^2 \rangle + \langle \mathbf{R}_{PP}^2 \rangle + 2\langle \mathbf{R}_{PE} \cdot \mathbf{R}_{PP} \rangle}{nl^2} \quad (2)$$

where l is the average backbone bond length (the same for both PE and PP blocks) and \mathbf{R}_{PE} and \mathbf{R}_{PP} are the end-to-end

vectors of PE and PP blocks as they are schematically shown in Figure 8.

Given that the characteristic ratios of PE and PP blocks, $C_{n_{PE}}^{PE}$ and $C_{n_{PP}}^{PP}$, are defined as

$$C_{n_{PE}}^{PE} = \frac{\langle \mathbf{R}_{PE}^2 \rangle}{n_{PE}l^2}, \quad C_{n_{PP}}^{PP} = \frac{\langle \mathbf{R}_{PP}^2 \rangle}{n_{PP}l^2} \quad (3)$$

respectively, and taking into account eq 1 and

$$x_{PE} = 1 - x_{PP} \quad (4)$$

we can transform eq 2 accordingly:

$$C_n^{PE-b-PP} = \frac{\langle \mathbf{R}_{PE}^2 \rangle + \langle \mathbf{R}_{PP}^2 \rangle + 2\langle \mathbf{R}_{PE} \cdot \mathbf{R}_{PP} \rangle}{nl^2} = \frac{\langle \mathbf{R}_{PE}^2 \rangle}{nl^2} + \frac{\langle \mathbf{R}_{PP}^2 \rangle}{nl^2} + 2\frac{\langle \mathbf{R}_{PE} \cdot \mathbf{R}_{PP} \rangle}{nl^2} = x_{PE}C_{n_{PE}}^{PE} + x_{PP}C_{n_{PP}}^{PP} + 2\frac{\langle \mathbf{R}_{PE} \cdot \mathbf{R}_{PP} \rangle}{nl^2} = (1 - x_{PP})C_{n_{PE}}^{PE} + x_{PP}C_{n_{PP}}^{PP} + 2\frac{\langle \mathbf{R}_{PE} \cdot \mathbf{R}_{PP} \rangle}{nl^2} \quad (5)$$

If we assume that the end-to-end vectors of PE and PP blocks are uncorrelated and thus $\langle \mathbf{R}_{PE} \cdot \mathbf{R}_{PP} \rangle = 0$, then the stiffness of the PE-*b*-PP chain is given by the following simple equation:

$$C_n^{PE-b-PP} = (1 - x_{PP})C_{n_{PE}}^{PE} + x_{PP}C_{n_{PP}}^{PP} \quad (6)$$

In Figure 9a–c we plot with red circles the sum $(1 - x_{pp})C_{nPE}^{PE} + x_{pp}C_{nPP}^{PP}$ as a function of x_{pp} . Here, we should note that C_{nPE}^{PE} and C_{nPP}^{PP} correspond to the characteristic ratio of the PE and PP blocks which consist of n_{PE} and n_{PP} backbone bonds, respectively, and not to the limiting values C_{∞}^{PE} and C_{∞}^{PP} . We note that our estimations of $C_n^{PE-b-PP}$, shown by the black squares, slightly deviate from the red circles which correspond to eq 6. The deviation comes from the fact that $\langle \mathbf{R}_{PE} \mathbf{R}_{PP} \rangle \neq 0$, and thus \mathbf{R}_{PE} and \mathbf{R}_{PP} are not fully uncorrelated. The latter is confirmed in the insets of Figure 9a–c, where $\frac{\langle \mathbf{R}_{PE} \mathbf{R}_{PP} \rangle}{nl^2}$ is plotted with green triangles against x_{pp} and we observe that $\frac{\langle \mathbf{R}_{PE} \mathbf{R}_{PP} \rangle}{nl^2} > 0$.

To examine if the latter is a system size effect, we have also performed additional MC simulations on systems with $n = n_{PE} + n_{PP} = 500, 1500, \text{ and } 2000$ backbone bonds. In Figure 9d, displaying the results of these simulations in the case of isotactic PP blocks, we note that, as we increase n , $\langle \mathbf{R}_{PE} \mathbf{R}_{PP} \rangle \rightarrow 0$, which means that the end-to-end vectors for very long PE and PP blocks become uncorrelated. Under these conditions, we can conclude that

$$C_{\infty}^{PE-b-PP} = (1 - x_{pp})C_{\infty}^{PE} + x_{pp}C_{\infty}^{PP} \quad (7)$$

In Figure 9a–c, we plot with blue lines eq 7, which finally corresponds to our predictions of $C_{\infty}^{PE-b-PP}$ for the PE-*b*-PP systems.

EPMs and *alt*-PEP. The last systems we study are five series of EPM chains with $p_m = 0, 0.3, 0.5, 0.7, \text{ and } 1$ as well as an alternating ethylene–propylene copolymer (*alt*-PEP) chain. Each EPM series consists of 9 EPM chains with $x_p = 0.1, 0.2, \dots, 0.9$ per mole of propylene units. All EPM and *alt*-PEP chains are chosen to have the same backbone length with the PE-*b*-PP ones, i.e., $n = 1000$. In the beginning, a series of EPM chains with $x_p = 0.1, 0.2, \dots, 0.9$ with $p_m = 1$ are generated, using the amorphous builder of MAPS suite.⁸⁹ Then, using a home-built program, we generated the remaining four EPM series with $p_m = 0, 0.3, 0.5$ and 0.7 , by simply rotating the methyl branches until the desired tacticity was achieved. Therefore, the sequence of ethylene and propylene units for a given x_p is the same for all p_m .

Single-chain MC simulations are performed on all EPM and *alt*-PEP chains for approximately 1 billion steps using the MC algorithm of Tzounis et al.⁹³ for various Δn_{pair} values to determine the optimum ones which maximize the stiffness of the chains. In Table 6, we present the optimum values of Δn_{pair} for each p_m and x_p for EPM chains.

Table 6. Δn_{pair} Values That Maximize C_{∞}^{EPM} for Each p_m and x_p for EPM Chains

x_p	p_m				
	0.0	0.3	0.5	0.7	1.0
0.1	2	2	2	2	2
0.2	2	2	2	2	2
0.3	2	2	2	2	2
0.4	2	2	2	2	2
0.5	2	2	2	2	2
0.6	2	2	2	2	2
0.7	2	2	2	2	3
0.8	2	2	2	2	3
0.9	2	2	2	2	3

The characteristic ratios C_n of all chains reach a plateau for high n values from which we can estimate the limiting C_{∞} value. In Figure 10a, we plot C_{∞}^{EPM} for the five series of EPM chains as a function of x_p with colored lines and symbols. We also denote with an orange star the C_{∞} value for *alt*-PEP ($x_p = 0.5$). For comparison, we have added the C_{∞} values of PE at $x_p = 0$ and PP at $x_p = 1$ for all the tacticities we studied, i.e., $p_m = 0, 0.3, 0.5, \text{ and } 0.7$. We note that at low x_p , as propylene content increases, C_{∞}^{EPM} immediately decreases, i.e., chains become less stiff, for all tacticities. The immediate drop of the stiffness corresponds to the presence of propylene units which destroy the all-*trans* sequences of the PE chains, leading them to less stiff conformations.

The decrease of C_{∞}^{EPM} is monotonic for $p_m = 0.5$ and 0.7 , while for $p_m = 0, 0.3, \text{ and } 1$ a minimum value appears, and then C_{∞}^{EPM} increases until it reaches the C_{∞} value of the corresponding PP homopolymer chain. In addition, the C_{∞}^{EPM} minimum does not appear at the same x_p . For $p_m = 0$ the minimum appears at approximately $x_p = 0.4$, while for $p_m = 0.3$ and 1 it appears at approximately $x_p = 0.8$. The nonmonotonic behavior of C_{∞}^{EPM} as a function of the propylene content of EPM chains has also been observed in the work of Mark,⁸⁶ where RIS calculations were performed on three different series of EPM chains with $p_m = 0, 0.5, \text{ and } 1$. For $p_m = 0$, Mark observed a minimum stiffness at $x_p = 0.5$, very close to our predictions, while for $p_m = 1$ he predicted minimum stiffness at $x_p = 0.6$, a little lower than our estimation of approximately $x_p = 0.8$. However, for $p_m = 0.5$ we do not observe a minimum C_{∞}^{EPM} , while Mark predicted a minimum stiffness at approximately $x_p = 0.8$. Finally, the stiffness of *alt*-PEP lies between our predictions of C_{∞}^{EPM} for $p_m = 0.3$ and $p_m = 0.5$.

A very interesting feature of Figure 10a is that for low propylene content, $x_p < 0.2$, all curves converge, having a common negative slope, while for $x_p > 0.2$ they begin to separate from each other. This effect indicates that for $x_p > 0.2$ the tacticity of the propylene unit sequences appearing along the EPM chains begins to affect stiffness and C_{∞}^{EPM} starts approaching the corresponding C_{∞}^{PP} value. To further investigate this effect, we plot in Figure 10b the fractions of PP dyads, triads, tetrads, and pentads along the EPM chains, $f_2, f_3, f_4, \text{ and } f_5$, respectively, as a function of x_p . We define f_q as the fraction of the number of propylene q -ads (dyad, triad, tetrad, pentad, etc.) along an EPM chain divided by the maximum number of propylene q -ads which could appear along the EPM chain for a given x_p . The latter maximum number equals the number of propylene q -ads present in a block copolymer of the same x_p where all PP units are adjacent.

We note that all fractions increase monotonically as x_p increases. However, for $x_p \leq 0.2$, $f_3, f_4, \text{ and } f_5$, denoted by red circles, green triangles, and blue diamonds, respectively, are very close to zero and only begin to increase for $x_p > 0.2$, indicating that tacticity begins to affect EPM chain stiffness as soon as PP sequences which consist of three, four, or five propylene units emerge.

Furthermore, the f_q fractions correspond to the probability of having $q - 1$ sequential propylene units immediately after a given propylene unit along an EPM chain. With Bernoullian statistics, one would expect $f_q = x_p^{q-1}$. In Figure 10b we plot with black, red, green, and blue solid lines the functions $f_q = x_p^{q-1}$ for $q = 2, 3, 4, \text{ and } 5$, respectively; we note that they are in perfect agreement with our simulation results.

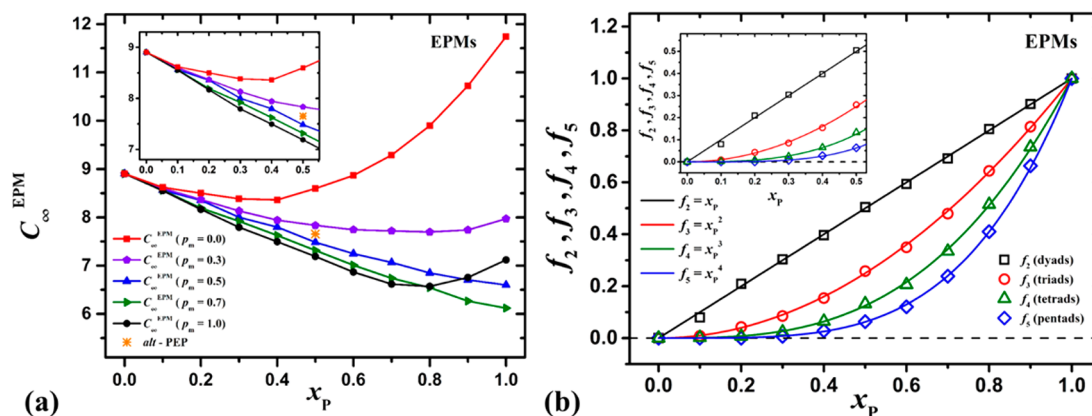


Figure 10. (a) Characteristic ratio, C_{∞}^{EPM} , for different EPM chains plotted as a function of the propylene content x_p . Red lines and symbols correspond to the system where all PP dyads are syndiotactic ($p_m = 0$), black to the system where all PP dyads are isotactic ($p_m = 1$), and purple, blue, and green lines and symbols correspond to the systems with $p_m = 0.3, 0.5$, and 0.7 , respectively. The orange star corresponds to the stiffness of an *alt*-PEP chain ($p_m = 0.5$). (b) Fraction of PP dyads, triads, tetrads, and pentads, f_2, f_3, f_4 , and f_5 , respectively, along an EPM chain plotted as a function of propylene content, x_p .

Table 7. Pre-Exponential Factor (A) and Exponent (B) Estimated by Fitting Equation $\langle R^2 \rangle_0/M = A \exp(-Bw_p)$ to Both Simulation and Experimental Results of $\langle R^2 \rangle_0/M$ in Figure 11 as a Function of w_p

method	T (K)	A	B ($\text{\AA}^2 \text{ mol g}^{-1}$)
MC simulations	348	1.74 ± 0.02	0.74 ± 0.02
SANS experiments ²³	348	1.33 ± 0.01	0.68 ± 0.01
MC simulations	413	1.58 ± 0.01	0.72 ± 0.01
SANS experiments ⁵⁸	413	1.25 ± 0.01	0.65 ± 0.02

Finally, in Figure 11 we plot in a semilog the unperturbed chain dimensions, expressed as a fraction of the mean-square

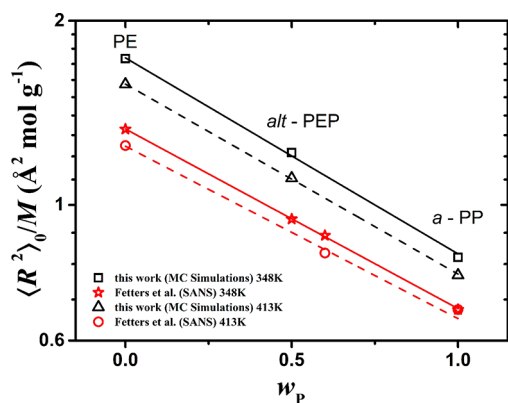


Figure 11. Semilog plot of the fraction of the mean-square end-to-end distance of a polymer chain, $\langle R^2 \rangle_0$, divided by the molar mass of the chain M , for the PE, *alt*-PEP, and *a*-PP chains as a function of the propylene weight fraction, w_p . Black lines and symbols correspond to the simulation results at both $T = 348$ and 413 K. Red lines and symbols correspond to SANS experimental measurements by Fetters et al.^{23,58} at both $T = 348$ and 413 K. Solid and dashed lines correspond to exponential decay fits to the corresponding simulation or experimental data.

end-to-end distance of a polymer chain, $\langle R^2 \rangle_0$, divided by the molar mass of the chain, M , for PE, *alt*-PEP, and *a*-PP chains, versus the propylene weight fraction w_p , at two different temperatures, $T = 348$ and 413 K. We compare our simulation results against the available experimental results. We note that

for both temperatures $\langle R^2 \rangle_0/M$ decays exponentially with w_p , i.e., $\langle R^2 \rangle_0/M = A \exp(-Bw_p)$ where A and B are free parameters. From the slopes of the fitted lines in Figure 11 we can estimate the pre-exponential factors A and the exponents B . As we note in Table 6, the exponents B estimated from our simulations are in very good agreement with the corresponding experimental results at both temperatures. However, all $\langle R^2 \rangle_0/M$ values from our simulations are systematically higher than the experimental ones. The latter is also reflected in the values of A extracted from our simulations, which are higher than the experimental ones. As we also discussed in the previous sections, this effect is attributable to TraPPE force field^{90–93,101–103} we apply and more specifically to its torsional potential which leads to stiffer chain conformations than in reality.^{92,93,101–103}

CONCLUSIONS

In this work we have performed a systematic study of the effects of tacticity on the unperturbed dimensions of polypropylene homopolymer systems as well as of ethylene-propylene copolymers. The first systems we studied were PP homopolymers with Bernoullian tacticity sequences and various fractions of *meso* dyads, p_m . We found that the stiffness of PP chains expressed by Flory's characteristic ratio, C_{∞} , displays a nonmonotonic behavior, having a minimum value at $p_m = 0.7$. Our results are in qualitative agreement with previous estimates from RIS calculations. In addition, by analyzing the torsional states of skeletal bonds, we identified the two competing processes which act simultaneously and cause the nonmonotonic dependence of C_{∞} versus p_m . Increasing p_m , on one hand, decreases the length of all-*trans* sequences along the chain, leading to a reduction in stiffness; on the other hand, it increases the length of helical *tgtg...* sequences, which contributes to an increase in stiffness. Next, we studied how tacticity and propylene content affect the stiffness of PE-*b*-PP copolymer chains, extracting a general relation that connects the stiffness of the PE-*b*-PP chains with the propylene content. The characteristic ratio of the block copolymer was found to be linear in the mole fraction of propylene units, x_p , in the limit of very long chains, for all PP block tacticities examined. Finally, we also studied how both tacticity and propylene content affect the stiffness of EPM

chains. We compared our results with the theoretical predictions of RIS models, and we found that they are in very good qualitative agreement; we also detected how the emergence of PP sequences longer than dyads along the EPM chains makes their stiffness sensitive to tacticity. The simulation and analysis methodology adopted in this study could be readily extended to future studies of the effects of tacticity and composition on the conformational properties of more complicated chiral polymers and copolymers such as polystyrene (PS) or poly(methyl methacrylate) (PMMA). In addition, one could examine the tacticity effects on physical properties such as the glass transition temperature or the self-diffusion coefficient using for example molecular dynamics simulations.

AUTHOR INFORMATION

Corresponding Author

*E-mail: doros@central.ntua.gr (D.N.T.).

ORCID

Panagiotis-Nikolaos Tzounis: 0000-0001-7824-6463

Stefanos D. Anogiannakis: 0000-0001-9766-2243

Doros N. Theodorou: 0000-0002-4763-9739

Notes

The authors declare no competing financial interest.

ACKNOWLEDGMENTS

We thank Professor Apostolos Kyritsis for fruitful discussions. Scienomics SARL is gratefully acknowledged for making their software available to us through the Scienomics Group of Scientific Excellence (SGSE) program. We are grateful to Mr. Vasilios D. Georgilas for his help with the generation of the initial configurations of EPM systems.

REFERENCES

- (1) Flory, P. J. On the Stereochemical Constitution and Nuclear Magnetic Resonance Spectra of Polypropylenes. *Macromolecules* **1970**, *3*, 613–617.
- (2) Hehn, M.; Maiko, K.; Pasch, H.; Hiller, W. Online HPLC–NMR: An Efficient Method for the Analysis of PMMA with Respect to Tacticity. *Macromolecules* **2013**, *46*, 7678–7686.
- (3) Stehling, F. C. Stereochemical configurations of polypropenes by high resolution nuclear magnetic resonance. *J. Polym. Sci., Part A: Gen. Pap.* **1964**, *2*, 1815–1823.
- (4) Cheng, H. N.; Kasehagen, L. J. Tacticity distribution and simulation. *Macromolecules* **1993**, *26*, 4774–4782.
- (5) Callan, J. F.; Fawcett, A. H.; Malcolm, R. K. The effect of tacticity on the conformational properties of poly(1-olefin sulfone)s. *J. Polym. Res.* **2008**, *15*, 107–113.
- (6) Sasanuma, Y.; Touge, D. Configurational statistics of poly(L-lactide) and poly(DL-lactide) chains. *Polymer* **2014**, *55*, 1901–1911.
- (7) Abu-Sharkh, B. F. Influence of tacticity on solubility of propene monomer in isotactic and syndiotactic polypropylene. *Polymer* **2004**, *45*, 6383–6389.
- (8) Tung, K.-L.; Lu, K.-T. Effect of tacticity of PMMA on gas transport through membranes: MD and MC simulation studies. *J. Membr. Sci.* **2006**, *272*, 37–49.
- (9) Lu, K.-T.; Tung, K.-L. Molecular dynamics simulation study of the effect of PMMA tacticity on free volume morphology in membranes. *Korean J. Chem. Eng.* **2005**, *22*, 512–520.
- (10) Haliloğlu, T.; Mattice, W. L. Detection of the onset of demixing in simulations of polypropylene melts in which the chains differ only in stereochemical composition. *J. Chem. Phys.* **1999**, *111*, 4327–4333.
- (11) Gupta, A. K.; Natarajan, U. Tacticity effects on the conformational structure and hydration of poly-(methacrylic acid)

in aqueous solutions—a molecular dynamics simulations study. *Mol. Simul.* **2016**, *42*, 725–736.

- (12) Fritz, D.; Harmandaris, V. A.; Kremer, K.; van der Vegt, N. F. A. Coarse-Grained Polymer Melts Based on Isolated Atomistic Chains: Simulation of Polystyrene of Different Tacticities. *Macromolecules* **2009**, *42*, 7579–7588.

- (13) Katsumoto, Y.; Kubosaki, N.; Miyata, T. Molecular Approach To Understand the Tacticity Effects on the Hydrophilicity of Poly(*N*-isopropylacrylamide): Solubility of Dimer Model Compounds in Water. *J. Phys. Chem. B* **2010**, *114*, 13312–13318.

- (14) Milano, G.; Müller-Plathe, F. Mapping Atomistic Simulations to Mesoscopic Models: A Systematic Coarse-Graining Procedure for Vinyl Polymer Chains. *J. Phys. Chem. B* **2005**, *109*, 18609–18619.

- (15) Behbahani, A. F.; Allaei, S. M. V.; Motlagh, G. H.; Eslamid, H.; Harmandaris, V. A. Structure and dynamics of stereo-regular poly(methyl-methacrylate) melts through atomistic molecular dynamics simulations. *Soft Matter* **2018**, *14*, 1449–1464.

- (16) von Meerwall, E.; Waheed, N.; Mattice, W. L. Effect of Stereochemistry on Diffusion of Polypropylene Melts: Comparison of Simulation and Experiment. *Macromolecules* **2009**, *42*, 8864–8869.

- (17) Chang, L.; Woo, E. M. Tacticity effects on glass transition and phase behavior in binary blends of poly(methyl methacrylate)s of three different configurations. *Polym. Chem.* **2010**, *1*, 198–202.

- (18) Geng, K.; Tsui, O. K. C. Effects of Polymer Tacticity and Molecular Weight on the Glass Transition Temperature of Poly(methyl methacrylate) Films on Silica. *Macromolecules* **2016**, *49*, 2671–2678.

- (19) Negash, S.; Tatek, Y. B.; Tsige, M. Effect of tacticity on the structure and glass transition temperature of polystyrene adsorbed onto solid surfaces. *J. Chem. Phys.* **2018**, *148*, 134705.

- (20) Arrighi, V.; Batt-Coutrot, D.; Zhang, C.; Telling, M. T. F.; Triolo, A. Effect of tacticity on the local dynamics of polypropylene melts. *J. Chem. Phys.* **2003**, *119*, 1271.

- (21) Lippow, S. M.; Qiu, X.; Ediger, M. D. Effect of tacticity on the segmental dynamics of polypropylene melts investigated by ¹³C nuclear magnetic resonance. *J. Chem. Phys.* **2001**, *115*, 4961.

- (22) Huang, C.-L.; Chen, Y. C.; Hsiao, T.-J.; Tsai, J.-C.; Wang, C. Effect of Tacticity on Viscoelastic Properties of Polystyrene. *Macromolecules* **2011**, *44*, 6155–6161.

- (23) Fetters, L. J.; Lee, J. H.; Mathers, R. T.; Hustad, P. D.; Coates, G. W.; Archer, L. A.; Rucker, S. P.; Lohse, D. J. Influence of Syndiotactic Propylene Units on the Rheological Parameters of Poly(ethylene-propylene) Copolymers. *Macromolecules* **2005**, *38*, 10061–10066.

- (24) Fetters, L. J.; Lohse, D. J.; Richter, D. J.; Witten, T. A.; Zirkel, A. Connection between Polymer Molecular Weight, Density, Chain Dimensions, and Melt Viscoelastic Properties. *Macromolecules* **1994**, *27*, 4639–4647.

- (25) Ahmad, N.; Di Girolamo, R.; Auriemma, F.; De Rosa, C.; Grizzuti, N. Relations between Stereoregularity and Melt Viscoelasticity of Syndiotactic Polypropylene. *Macromolecules* **2013**, *46*, 7940–7946.

- (26) Chile, L.-E.; Mehrkhodavandi, P.; Hatzikiriakos, S. G. A Comparison of the Rheological and Mechanical Properties of Isotactic, Syndiotactic, and Heterotactic Poly(lactide). *Macromolecules* **2016**, *49*, 909–919.

- (27) Eckstein, A.; Suhm, J.; Friedrich, C.; Maier, R.-D.; Sassmannshausen, J.; Bochmann, M.; Mühlaupt, R. Determination of Plateau Moduli and Entanglement Molecular Weights of Isotactic, Syndiotactic, and Atactic Polypropylenes Synthesized with Metallocene Catalysts. *Macromolecules* **1998**, *31*, 1335–1340.

- (28) Rwei, S.-P.; Way, T.-F.; Chiang, W.-Y.; Pan, S.-Y. Effect of tacticity on the cyclization of polyacrylonitrile copolymers. *Colloid Polym. Sci.* **2017**, *295*, 803–815.

- (29) Paukkeri, R.; Lehtinen, A. Thermal behaviour of polypropylene fractions: 1. Influence of tacticity and molecular weight on crystallization and melting behaviour. *Polymer* **1993**, *34*, 4075–4082.

- (30) Choi, D.; White, J. L. Crystallization and orientation development in fiber and film processing of polypropylenes of

varying stereoregular form and tacticity. *Polym. Eng. Sci.* **2004**, *44*, 210–222.

(31) Min, K. E.; Paul, D. R. Effect of tacticity on permeation properties of poly(methyl methacrylate). *J. Polym. Sci. B* **1988**, *26*, 1021–1033.

(32) Beaucage, G.; Stein, R. S.; Hashimoto, T.; Hasegawa, H. Tacticity effects on polymer blend miscibility. *Macromolecules* **1991**, *24*, 3443–3448.

(33) Beaucage, G.; Stein, R. S.; Koningsveld, R. Tacticity effects on polymer blend miscibility. 1. Flory-Huggins-Staverman analysis. *Macromolecules* **1993**, *26*, 1603–1608.

(34) Beaucage, G.; Stein, R. S. Tacticity effects on polymer blend miscibility. 2. Rate of phase separation. *Macromolecules* **1993**, *26*, 1609–1616.

(35) Beaucage, G.; Stein, R. S. Tacticity Effects on Polymer Blend Miscibility. 3. Neutron Scattering Analysis. *Macromolecules* **1993**, *26*, 1617–1626.

(36) Honeycutt, J. D. A. Theoretical Study of Tacticity Effects on Poly(vinyl chloride)/Poly(methyl methacrylate) Miscibility. *Macromolecules* **1994**, *27*, 5377–5381.

(37) Seki, M.; Nakano, H.; Yamauchi, S.; Suzuki, J.; Matsushita, Y. Miscibility of Isotactic Polypropylene/Ethylene-Propylene Random Copolymer Binary Blends. *Macromolecules* **1999**, *32*, 3227–3234.

(38) Kamdar, A. R.; Hu, Y. S.; Ansems, P.; Chum, S. P.; Hiltner, A.; Baer, E. Miscibility of Propylene–Ethylene Copolymer Blends. *Macromolecules* **2006**, *39*, 1496–1506.

(39) Alberdi, M.; Espi, E.; Fernandez-Berridi, M. J.; Iruin, J. J. Influence of the Blending Method and Poly(methyl methacrylate) Tacticity in Its Miscibility with Poly(hydroxy ether of bisphenol A, phenoxy). *Polym. J.* **1994**, *26*, 1037–1046.

(40) Takhulee, A.; Vao-Soongnern, V. Monte Carlo simulation study of the effect of chain tacticity on demixing of polyethylene/polypropylene blends. *Polym. Sci., Ser. A* **2014**, *56*, 936–944.

(41) Maier, R.-D.; Thomann, R.; Kressler, J.; Müllhaupt, R.; Rudolf, B. The influence of stereoregularity on the miscibility of poly(propylene)s. *J. Polym. Sci., Part B: Polym. Phys.* **1997**, *35*, 1135–1144.

(42) Shih, H.-Y.; Kuo, W. F.; Pearce, E. M.; Kwei, T. K. Tacticity effects on the miscibility behavior of poly(methyl methacrylate)/poly(ethylene oxide-*b*-dimethylsiloxane-*b*-ethylene oxide) blends. *J. Polym. Res.* **1995**, *2*, 147–154.

(43) Hsu, W.-P. Effect of tacticity of poly(methyl methacrylate) on the miscibility with poly(vinyl pyrrolidone). *J. Appl. Polym. Sci.* **2001**, *81*, 3190–3197.

(44) Su, W.-F. Structure Morphology Flow of Polymer. In *Principles of Polymer Design and Synthesis*; Springer-Verlag: Berlin, 2013; pp 27–59.

(45) Feng, H.; Lu, X.; Wang, W.; Kang, N.-G.; Mays, J. W. Block Copolymers: Synthesis, Self-Assembly, and Applications. *Polymers* **2017**, *9*, 494.

(46) Li, X.; Liu, Y.; Wan, L.; Li, Z.; Suh, H.; Ren, J.; Ocola, L. E.; Hu, W.; Ji, S.; Nealey, P. F. Effect of Stereochemistry on Directed Self-Assembly of Poly(styrene-*b*-lactide) Films on Chemical Patterns. *ACS Macro Lett.* **2016**, *5*, 396–401.

(47) Isono, T.; Lee, H.; Miyachi, K.; Satoh, Y.; Kakuchi, T.; Ree, M.; Satoh, T. Synthesis, Thermal Properties, and Morphologies of Amphiphilic Brush Block Copolymers with Tacticity-Controlled Polyether Main Chain. *Macromolecules* **2018**, *51*, 2939–2950.

(48) Davidson, E. C.; Rosales, A. M.; Patterson, A. L.; Russ, B.; Yu, B.; Zuckermann, R. N.; Segalman, R. A. Impact of Helical Chain Shape in Sequence-Defined Polymers on Polypeptoid Block Copolymer Self-Assembly. *Macromolecules* **2018**, *51*, 2089–2098.

(49) Williams, A. D.; Flory, P. J. Stereochemical equilibrium and configurational statistics in polystyrene and its oligomers. *J. Am. Chem. Soc.* **1969**, *91*, 3111–3118.

(50) Zhou, Z.; Yan, D. Configurational-conformational statistics of stereoirregular polystyrene. *Macromol. Theory Simul.* **1996**, *5*, 939–945.

(51) Sundararajan, P. R. Conformational Analysis of Poly(methyl methacrylate). *Macromolecules* **1986**, *19*, 415–421.

(52) Yan, D.; Zhou, Z. Configurational-conformational statistics of stereoirregular poly(methyl methacrylate)s. *J. Macromol. Sci., Part B: Phys.* **1999**, *38*, 217–225.

(53) Sasanuma, Y.; Touge, D. Configurational statistics of poly(L-lactide) and poly(DL-lactide) chains. *Polymer* **2014**, *55*, 1901–1911.

(54) Fetters, L. J.; Graessley, W. W.; Krishnamoorti, R.; Lohse, D. J. Melt Chain Dimensions of Poly(ethylene - 1-butene) Copolymers via Small Angle Neutron Scattering. *Macromolecules* **1997**, *30*, 4973–4977.

(55) Smith, G. D.; Yoon, D. Y.; Jaffe, R. L.; Colby, R. L.; Krishnamoorti, R.; Fetters, L. J. Conformations and Structures of Poly(oxyethylene) Melts from Molecular Dynamics Simulations and Small-Angle Neutron Scattering Experiments. *Macromolecules* **1996**, *29*, 3462–3469.

(56) Xu, Z.; Hadjichristidis, N.; Carella, J. M.; Fetters, L. J. Characteristic Ratios of Atactic Poly(vinylethylene) and Poly(ethylene). *Macromolecules* **1983**, *16*, 925–929.

(57) Xu, Z.; Hadjichristidis, N.; Fetters, L. J.; Mays, J. W. Structure/chain-flexibility relationships of polymers; In *Physical Properties of Polymers*; Springer: Berlin, 1995; pp 1–50.

(58) Fetters, L. J.; Lohse, D. J.; Garcia-Franco, C. A.; Brant, P.; Richter, D. Prediction of Melt State Poly(α -olefin) Rheological Properties: The Unsuspected Role of the Average Molecular Weight per Backbone Bond. *Macromolecules* **2002**, *35*, 10096–10101.

(59) Fetters, L. J.; Lohse, D. J.; Graessley, W. W. Chain Dimensions and Entanglement Spacings in Dense Macromolecular Systems. *J. Polym. Sci., Part B: Polym. Phys.* **1999**, *37*, 1023–1033.

(60) Li, W.; Nealey, P. F.; de Pablo, J. J.; Müller, M. Defect Removal in Course of Directed Self-Assembly is Facilitated in the Vicinity of the Order-Disorder Transition. *Phys. Rev. Lett.* **2014**, *113*, 168301.

(61) Hur, S.-M.; Khaira, G. S.; Ramírez-Hernández, A.; Müller, M.; Nealey, P. F.; de Pablo, J. J. Simulation of Defect Reduction in Block Copolymer Thin Films by Solvent Annealing. *ACS Macro Lett.* **2015**, *4*, 11–15.

(62) Hill, J. D.; Millett, P. C. Numerical Simulations of Directed Self-Assembly in Diblock Copolymer Films using Zone Annealing and Pattern Templating. *Sci. Rep.* **2017**, *7*, 5250.

(63) Hebbeker, P.; Steinschulte, A. A.; Schneider, S.; Okuda, J.; Möller, M.; Plamper, F. A.; Schneider, S. Complexation in Weakly Attractive Copolymers with Varying Composition and Topology: Linking Fluorescence Experiments and Molecular Monte Carlo Simulations. *Macromolecules* **2016**, *49*, 8748–8757.

(64) Müller, M.; Orozco Rey, J. C. Continuum models for directed self-assembly. *Mol. Syst. Des. Eng.* **2018**, *3*, 295–313.

(65) Bates, F. S.; Fredrickson, G. H. Block Copolymer Thermodynamics: Theory and Experiment. *Annu. Rev. Phys. Chem.* **1990**, *41*, 525–557.

(66) Vavasour, J. D.; Whitmore, M. D. Self-consistent field theory of block copolymers with conformational asymmetry. *Macromolecules* **1993**, *26*, 7070–7075.

(67) Vavasour, J. D.; Whitmore, M. D. Self-consistent mean field theory of the microphases of diblock copolymers. *Acta Polym.* **1995**, *46*, 341–360.

(68) Zhang, L.; Lin, J.; Lin, S. Effect of Molecular Architecture on Phase Behavior of Graft Copolymers. *J. Phys. Chem. B* **2008**, *112*, 9720–9728.

(69) Li, J.; Zhang, H.; Qiu, F. Self-consistent field theory of block copolymers on a general curved surface. *Eur. Phys. J. E: Soft Matter Biol. Phys.* **2014**, *37*, 18.

(70) Brückner, S.; Allegra, G.; Corradini, P. Helix Inversions in Polypropylene and Polystyrene. *Macromolecules* **2002**, *35*, 3928–3936.

(71) Yamamoto, T.; Sawada, K. Molecular-dynamics simulation of crystallization in helical polymers. *J. Chem. Phys.* **2005**, *123*, 234906.

(72) Androsch, R.; Di Lorenzo, M. L.; Schick, C.; Wunderlich, B. Mesophases in polyethylene, polypropylene, and poly(1-butene). *Polymer* **2010**, *51*, 4639–4662.

- (73) Biskup, U.; Cantow, H.-J. Calculations on the Unperturbed Dimensions of Polypropylenes. *Macromolecules* **1972**, *5*, 546–550.
- (74) Suter, U. W.; Flory, P. J. Conformational Energy and Configurational Statistics of polypropylene. *Macromolecules* **1975**, *8*, 765–776.
- (75) Boyd, R. H.; Breiting, S. M. Conformational Properties of Polypropylene. *Macromolecules* **1972**, *5*, 279–286.
- (76) Theodorou, D. N.; Suter, U. W. Shape of Unperturbed Linear Polymers: Polypropylene. *Macromolecules* **1985**, *18*, 1206–1214.
- (77) Zhou, Z.; Yang, W.; Yan, D.; Liu, H. Temperature Dependence of Polypropylene Configurations. *Macromol. Theory Simul.* **2014**, *23*, 76–83.
- (78) Jones, T. D.; Chaffin, K. A.; Bates, F. S.; Annis, B. K.; Hagaman, e. W.; Kim, M.-H.; Wignall, G. D.; Fan, W.; Waymouth, R. Effect of Tacticity on Coil Dimensions and Thermodynamic Properties of Polypropylene. *Macromolecules* **2002**, *35*, 5061–5068.
- (79) Kinsinger, J. B.; Hughes, R. E. The Unperturbed Dimensions of Atactic and Isotactic Polypropylene. *J. Phys. Chem.* **1963**, *67*, 1922–1923.
- (80) Antoniadis, S. J.; Samara, C. T.; Theodorou, D. N. Effect of Tacticity on the Molecular Dynamics of Polypropylene Melts. *Macromolecules* **1999**, *32*, 8635–8644.
- (81) Theodorou, D. N. Variable Connectivity Monte Carlo Algorithms for the Atomistic Simulation of Long-Chain Polymer Systems. In *Bridging Time Scales: Molecular Simulations for the Next Decade*; Lecture Notes in Physics 605; Nielaba, P., Mareschal, M., Ciccotti, G., Eds.; Springer-Verlag: Berlin, 2002; pp 67–127.
- (82) Tian, J.; Hustad, P. D.; Coates, G. W. A New Catalyst for Highly Syndiospecific Living Olefin Polymerization: Homopolymers and Block Copolymers from Ethylene and Propylene. *J. Am. Chem. Soc.* **2001**, *123*, 5134–5135.
- (83) Mead, J. L.; Tao, Z.; Liu, H. S. Insulation Materials for Wire and Cable Applications. *Rubber Chem. Technol.* **2002**, *75*, 701–712.
- (84) Baldwin, F. P.; Ver Strate, G. Polyolefin Elastomers Based on Ethylene and Propylene. *Rubber Chem. Technol.* **1972**, *45*, 709–881.
- (85) Gahleitner, M.; Jääskeläinen, P.; Ratajski, E.; Paulik, C.; Reussner, J.; Wolfschwenger, J.; Neißl, W. Propylene–ethylene random copolymers: Comonomer effects on crystallinity and application properties. *J. Appl. Polym. Sci.* **2005**, *95*, 1073–1081.
- (86) Mark, J. E. On the Configurational Statistics of Ethylene-Propylene Copolymers. *J. Chem. Phys.* **1972**, *57*, 2541–2548.
- (87) Mays, J. W.; Fetters, L. J. Temperature coefficients of unperturbed dimensions for atactic polypropylene and alternating poly(ethylene-propylene). *Macromolecules* **1989**, *22*, 921–926.
- (88) Zirkel, A.; Richter, D.; Pyckhout-Hintzen, W.; Fetters, L. J. Temperature dependence of the unperturbed dimensions of alternating poly(ethylene-propylene). *Macromolecules* **1992**, *25*, 954–960.
- (89) *Scienomics*, MAPS platform: version 3.4.1, France, 2014.
- (90) Wick, D. C.; Martin, G. C.; Siepmann, J. I. Transferable Potentials for Phase Equilibria. 4. United-Atom Description of Linear and Branched Alkenes and Alkylbenzenes. *J. Phys. Chem. B* **2000**, *104*, 8008–8016.
- (91) Pütz, M.; Curro, J. G.; Grest, G. S. Self-consistent integral equation theory of polyolefins: comparison to molecular dynamics simulations and x-ray scattering. *J. Chem. Phys.* **2001**, *114*, 2847–2860.
- (92) Heine, D.; Wu, D. T.; Curro, J. G.; Grest, G. S. Role of intramolecular energy on polyolefin miscibility: Isotactic polypropylene/polyethylene blends. *J. Chem. Phys.* **2003**, *118*, 914–924.
- (93) Tzounis, P.-N.; Anogiannakis, S. D.; Theodorou, D. N. General Methodology for Estimating the Stiffness of Polymer Chains from Their Chemical Constitution: A Single Unperturbed Chain Monte Carlo Algorithm. *Macromolecules* **2017**, *50*, 4575–4587.
- (94) Flory, P. J. *Principles of Polymer Chemistry*; Cornell University Press: Ithaca, NY, 1986.
- (95) Zirkel, A.; Urban, V.; Richter, D.; Fetters, L. J.; Huang, J. S.; Kampmann, R.; Hadjichristidis, N. Small-Angle Neutron Scattering Evaluation of the Temperature Dependence of Atactic Polypropylene and Poly(1-butene) Chain Dimensions in the Melt. *Macromolecules* **1992**, *25*, 6148–6155.
- (96) Fetters, L. J.; Lohse, D. J.; Colby, R. H. Chain dimensions and entanglement spacing. In *Physical Properties of Polymers Handbook*; Mark, J. E., Ed.; Springer: New York, 2007; pp 447–454.
- (97) Logotheti, G. E.; Theodorou, D. N. Segmental and Chain Dynamics of Isotactic Polypropylene Melts. *Macromolecules* **2007**, *40*, 2235–2245.
- (98) Romanos, N. A.; Theodorou, D. N. Crystallization and Melting Simulations of Oligomeric $\alpha 1$ Isotactic Polypropylene. *Macromolecules* **2010**, *43*, 5455–5469.
- (99) Romanos, N. A.; Theodorou, D. N. Melting Point and Solid–Liquid Coexistence Properties of $\alpha 1$ Isotactic Polypropylene as Functions of Its Molar Mass: A Molecular Dynamics Study. *Macromolecules* **2016**, *49*, 4663–4673.
- (100) Toxvaerd, S. Equation of state of alkanes II. *J. Chem. Phys.* **1997**, *107*, 5197–5204.
- (101) Uhlherr, A.; Doxastakis, M.; Mavrantzas, V. G.; Theodorou, D. N.; Leak, S. J.; Adam, N. E.; Nyberg, P. E. Atomic structure of a high polymer melt. *Europhys. Lett.* **2002**, *57*, 506–511.
- (102) Martins, J. A.; Micaelo, N. M. Short-Range Order in Polyethylene Melts: Identification and Characterization. *Macromolecules* **2013**, *46*, 7977–7988.
- (103) Ramos, J.; Vega, J. F.; Martínez-Salazar, J. Predicting experimental results for polyethylene by computer simulation. *Eur. Polym. J.* **2018**, *99*, 298–331.
- (104) Connolly, R.; Bellesia, G.; Timoshenko, E. G.; Kuznetsov, Y. A.; Elli, S.; Ganazzoli, F. Intrinsic and “Topological” Stiffness in Branched Polymers. *Macromolecules* **2005**, *38*, 5288–5299.
- (105) Elli, S.; Ganazzoli, F.; Timoshenko, E. G.; Kuznetsov, Y. A.; Connolly, R. Size and persistence length of molecular bottle-brushes by Monte Carlo simulations. *J. Chem. Phys.* **2004**, *120*, 6257–6267.
- (106) Yethiraj, A. A Monte Carlo simulation study of branched polymers. *J. Chem. Phys.* **2006**, *125*, 204901.
- (107) Xu, Z.; Mays, J.; Chen, X.; Hadjichristidis, N.; Schilling, F. C.; Bair, H. E.; Pearson, F. C.; Fetters, L. J. Molecular Characterization of Poly(2-methyl-1,3-pentadiene) and Its hydrogenated Derivative, Atactic Polypropylene. *Macromolecules* **1985**, *18*, 2560–2566.
- (108) Allegra, G.; Brückner, S. Copolymer Chain Statistics. The Pseudo-Stereochemical Equilibrium Approach within the Continuum of Rotational States. The Unperturbed Dimensions of Atactic Polypropylene. *Macromolecules* **1977**, *10*, 106–113.
- (109) Alfonso, G. C.; Yan, D.; Zhou, Z. Configurational-Conformational Statistics of atactic Polypropylene. *Polymer* **1993**, *34*, 2830–2835.
- (110) Ballard, D. G. H.; Cheshire, P.; Longman, G. W.; Schelten, J. Small-angle neutron scattering studies of isotropic polypropylene. *Polymer* **1978**, *19*, 379–385.